

# The Influence of Cold Deformation and Annealing on Texture Changes in Austenitic Stainless Steel

Joanna Kowalska<sup>1\*</sup>, Małgorzata Witkowska<sup>1</sup>

<sup>1</sup> Faculty of Metals Engineering and Industrial Computer Science, AGH University of Krakow, Al. Mickiewicza 30, 30-059 Kraków, Poland

\* Corresponding author's e-mail: joannak@agh.edu.pl

## ABSTRACT

Austenitic stainless steels are widely used in industry, from heavy industry and power generation to precision mechanics and electronics, accounting for about 2/3 of the stainless steels produced. The stability of austenite influences the properties and behaviour of these steels during deformation and annealing. This paper presents the results of research into austenitic metastable phase X5CrNi1810 steel, which was subjected to cold rolling (in the range of 5 to 80%) and then annealing (at temperatures of 500–900 °C). The research focused mainly on changes in crystallographic texture parameters occurring during the analysed processes. It was found that the observed development of the deformation texture is complex due to the fact that several processes take place simultaneously. Namely, the deformation of austenite, the transformation of austenite into martensite, and the deformation of the resulting martensite. The texture of the deformed austenite was similar to the texture of the alloy type  $\{112\}\langle 110 \rangle$ . After 80% deformation, the Goss-type  $\{110\}\langle 001 \rangle$  texture component showed the highest intensity. The lack of  $\{112\}\langle 111 \rangle$  orientation in the texture was due to the fact that this orientation changes to the  $\{112\}\langle 110 \rangle$  martensite orientation as a result of the  $\gamma \rightarrow \alpha'$  phase transition. Annealing of the deformed steel at 500 °C led to an increase in the degree of texturing (sharpening of the texture), which was related to the improvement of the texture in this temperature range. Above 600 °C, the degree of texturing decreased, which is directly related to the  $\alpha' \rightarrow \gamma$  reverse transformation and the subsequent recrystallization process. Magnetic studies indicate an increasing proportion of the magnetic phase  $\alpha'$  (martensite) together with an increasing degree of deformation. For deformation of 80%, the amount of magnetic phase reached a value of more than 33%. After annealing at a temperature of 800 °C, there is no martensite in the structure, which indicates that, in these heat treatment conditions, the complete reverse transformation of martensite into austenite has already taken place.

**Keywords:** crystallographic texture; austenite; martensite; phase transformation.

## INTRODUCTION

The group of corrosion-resistant steels includes austenitic steels. They were patented over 100 years ago, specifically in 1912, by the German Krupp engineers. However, it should be noted that these steels were discovered independently in England and Germany, when it was observed that the addition of chromium to iron prevents corrosion in humid air, and the introduction of nickel stabilizes the austenite structure to room temperature [1]. Austenitic steels constitute about 70% of

the stainless steels currently produced [2]. These steels generally contain 17–25% Cr, 8–39% Ni, a maximum of 0.1% C, and, depending on the type, additions of such elements as N, Mo, Mn and Si [3–5]. In addition to austenite,  $\delta$ -ferrite (up to 10%) may also be present in the structure, but they are still classified as austenitic steels [3, 6]. The presence of  $\delta$ -ferrite leads to an increase in the strength properties of these alloys [3]. Austenitic stainless steels are among the engineering materials with the most universal applications. Due to their good mechanical properties, corrosion

resistance at both elevated and lower temperatures, as well as biocompatibility, they are widely used in the chemical and petrochemical, energy and nuclear, aviation, transport, pharmaceutical, food, construction and medical industries [7–9]. Austenitic stainless steels, like other stainless steels, can be processed by forging, rolling, pressing or drawing, both cold and hot (recommended processing temperature of 955–1140 °C) [1]. Due to the fact that they have a single-phase structure, they cannot be strengthened by heat treatment but only by cold plastic deformation [10, 11]. Annealing of these steels after deformation may lead to the formation of carbides and intermetallic phases [12]. An important structural effect occurring in steels with an austenitic structure Cr-Ni [13–15] and high-manganese steels [16–18] is the occurrence of a phase transformation during cold plastic deformation, called the TRIP (TRansformation Induced Plasticity) effect and mechanical twinning (called the TWIP effect) [19]. The deformation-induced martensitic transformation is influenced by many factors, such as: temperature, the degree and method of deformation, as well as the chemical composition, size and crystallographic orientation of the austenite grain [20, 21]. The instability of austenite depends on the stacking fault energy (SFE), which is influenced by the chemical composition and temperature [22–24]. If the steel was deformed below the temperature  $M_{d30/50}$  then a phase transformation induced by deformation took place in the steel.  $M_{d30/50}$  is the temperature at which, after 30% deformation, 50% martensite forms in the structure. This is higher than the temperature  $M_s$  ( $M_s$  – temperature at which austenite begins its transformation into martensite during cooling) [12, 25, 26]. Two types of martensite can be formed in metastable austenitic steels: paramagnetic  $\epsilon$ -martensite with a hexagonal closed packed structure and ferromagnetic  $\alpha'$ -martensite with a body-centered cubic (BCC) structure [12, 25]. Padilha et al. [25] observed that  $\epsilon$ -martensite was formed in AISI 304 austenitic steel at low degrees of deformation up to 5% and then transformed into  $\alpha'$ -martensite. As a result of plastic deformation in austenite, the density of dislocations increases, which also resulted in an increase in the volume fraction of stacking faults (SF). For a regular face-centered cubic structure (FCC), SF have a hexagonal symmetry, like  $\epsilon$ -martensite. Therefore,  $\epsilon$ -martensite nucleates on SF. In general, the course of deformation-induced transformations can be written

as  $\gamma \rightarrow SF \rightarrow nSF \rightarrow \epsilon \rightarrow \alpha'$  [26]. As the temperature decreases, so does the SFE, which favors the transformation of  $\gamma$ -austenite into martensite and leads to the formation of more martensite [6]. This has also been confirmed in high-manganese austenitic steels [18, 27, 28]. Literature data indicate that if the  $\gamma$ -austenite stacking fault energy  $\gamma SFE \geq 45$  mJ/m<sup>2</sup> then cross slip is active, and during deformation a dislocation substructure is formed, which ultimately leads to the formation of  $\alpha'$ -martensite [29]. If  $\gamma SFE < 45$  mJ/m<sup>2</sup> the dominant deformation mechanism is twinning and deformation bands are formed, leading to the formation of  $\epsilon$ -martensite, which, if  $\gamma SFE < 18$  mJ/m<sup>2</sup>, is transformed into  $\alpha'$ -martensite [30]. To sum up, the transformation of austenite into martensite may occur by the transformation  $\gamma \rightarrow \epsilon$ ,  $\gamma \rightarrow \epsilon \rightarrow \alpha'$  or directly by  $\gamma \rightarrow \alpha'$  [31–33].

The recrystallization process of austenitic steel in which a phase transformation occurred during deformation is more complex. During annealing, the  $\epsilon \rightarrow \gamma$  and  $\alpha' \rightarrow \gamma$  reverse transformation of martensite ( $\epsilon$  and  $\alpha'$ ) into austenite ( $\gamma$ ) occurs [34–36]. The reverse transformation therefore precedes the subsequent stages of recrystallization. Padilha et al. [25], Martins et al. [37] and Tavares et al. [38] report that the reverse transformation of deformation-induced martensite into austenite exhibits two components: an athermal shear mechanism and an isothermal diffusion mechanism. Takaki et al. [39] showed that if steel with strongly defective martensite is annealed, as a result of the reverse transformation, austenite nuclei will be formed in random places of the recovered martensitic matrix, and after transformation, a fine austenite grain with a size smaller than 1  $\mu\text{m}$  can be obtained.

As a result of deformation and annealing, a crystallographic texture is created in metals and alloys with a regular face-centered cubic structure (FCC), which is influenced by SFE. In metals and alloys with a regular FCC, there are two types of rolling texture, namely alloy and pure metal. Additionally, a transitional texture is also observed. If SFE is lower than 40 mJ/m<sup>2</sup> then the typical deformation texture is an alloy type  $\{110\}\langle 112 \rangle$  texture [40]. If the SFE of the metal or alloy is large, i.e.,  $EBU > 70$  mJ/m<sup>2</sup>, then, as a result of deformation, a pure metal-type  $\{112\}\langle 111 \rangle$  texture (Cu-type) is created. In most cases, in the texture of cold-rolled metals and alloys with the FCC structure and in austenitic steels after large degrees of deformation, the dominant orientation was

{110}<112> (brass-type) and the weaker orientations were {110}<001> and {112}<111>, which depended primarily on the SFE value [41–43]. The texture changes that occur during annealing depend on the texture of the material after deformation and the annealing conditions (temperature and time). During recovery, no significant changes in the material texture are observed. Annealing at higher temperatures leads to the development of typical recrystallization textures, and the texture components of the deformed material are preserved in only a few cases. Donadille et al. [42] justified this effect by the chemical composition of steel (mainly due to the influence of molybdenum) and the resulting recrystallization process. The obtained results were interpreted as the result of oriented nucleation in shear bands of {110}<100> oriented grains, which grow into {111}<uvw> areas, and the deceleration of further oriented growth through the strong influence of molybdenum.

The aim of this work is a comprehensive analysis of the global crystallographic texture of the austenitic matrix and the texture of martensite induced by plastic deformation in metastable austenitic steel, which was created as a result by cold rolling and then during annealing.

## MATERIALS AND METHODS

The subject of the research was chrome-nickel AISI 304 austenitic stainless steel. The chemical composition of the steel was determined using a Foundry-Master optical emission spectrometer (Table 1). The steel came from industrial smelting.

After hot rolling, the steel was cut. Then, samples with dimensions of 9.95×20×150 mm were cold rolled in laboratory conditions to a deformation range of approximately 5–80%. After 80% deformation, the material was then annealed at the temperatures of 500 °C, 600 °C, 700 °C, 800 °C and 900 °C for 1 hour and cooled in water. Based on formula 1 [44], the engineering

deformation ( $\epsilon$ ) was calculated for the tested steel and the results are presented in Table 2.

$$\epsilon = \frac{\Delta h}{h_o} \cdot 100\% \tag{1}$$

where:  $\Delta h = h_o - h_n$ ,  $\epsilon$  – engineering deformation [%],  $h_o$  – output band thickness [mm],  $h_n$  – band thickness after a certain degree of deformation [mm].

Using appropriate empirical formulas 2 and 3 proposed by Padilha et al. [25] the stacking fault energy (SFE) for steel and the deformation-induced martensitic transformation temperature  $M_{d30/50}$  were calculated and equaled 17.13 mJ/m<sup>2</sup> and 41,42 °C, respectively

$$\text{SFE (mJ/m}^2\text{)} = -53 + 6.2(\%Ni) + 0.7(\%Cr) + 3.2(\%Mn) + 9.3(\%Mo) \tag{2}$$

$$M_{d30/50} (\text{°C}) = 413 - [462(\%C + \%N) + 9.2(\%Si) + 8.1(\%Mn) + 13.7(\%Cr) + 9.5(\%Ni) + 18.5(\%Mo)] \tag{3}$$

X-ray qualitative phase analysis was performed on a Siemens D500 diffractometer using monochromatic radiation from a tube with a copper anode of  $\lambda_{K\alpha} = 0.154$  nm, with the step counting method in the range  $2\theta = 35\text{--}110^\circ$  and steps  $\Delta 2\theta = 0.02^\circ$ , counted in the range = 5 seconds/step. The crystallographic texture was measured on a Bruker D8 Advance diffractometer using radiation from a tube with a cobalt anode of  $\lambda_{K\alpha} = 0.179$  nm. Incomplete pole figures of the planes {111} $\gamma$ , {200} $\gamma$ , {220} $\gamma$  and {311} $\gamma$  for austenite as well as {110} $\alpha$ , {200} $\alpha$  and {211} $\alpha$  for  $\alpha'$ -martensite were recorded. Then, on their basis, the orientation distribution function (ODF) and orientation fibers were calculated. The volume fractions of individual components present in the austenite

**Table 2.** Band thickness and calculated engineering deformation for cold rolled austenitic stainless steel

Thickness [mm]	9.95	9.45	7.85	6.02	4	2.05
$\epsilon$ [%]	0	5	20	40	60	80

**Table 1.** Chemical composition of austenitic stainless steel (in weight %)

Examined chemical composition							
Cr	Ni	C	Mn	Si	P	S	Fe
19.75	8.21	0.016	1.69	0.21	0.027	0.006	Balance
Chemical composition AISI 304 steel (1.4301)							
17.5/19.5	8/10.5	0.07	Max 2	Max 0.75	Max 0.0045	Max 0.03	Balance

and martensite texture were calculated using the LaboTex3 computer program. The program loads pole figures from files saved in the .epf format. The orientation distribution function (ODF) is then computed from the pole figures. Knowledge of this function enables the calculation of the percentages of selected crystallographic orientation components.

Samples for diffraction tests (size 20×15 mm) were prepared by grinding on water-based abrasive papers with grades from 300 to 2000, and polishing with diamond pastes (9, 6 and 3 μm). The samples were then electropolished to remove the deformed layer. The electrolyte composition was as follows: perchloric acid 80 cm<sup>3</sup>, ethanol 700 cm<sup>3</sup>, distilled water 120 cm<sup>3</sup>, and butoxy-ethanol 100 cm<sup>3</sup>. The surface layer of the sheets was tested. Effective penetration depth for Bragg-Brentano geometry in the angular range 2θ = 35 – 110° was from 2.18 to 5.87 μm.

Metallographic observations were performed using a Leica DM4000M light microscope. Longitudinal sections of the sheets were analyzed (length 15 mm). Metallographic sections were made by grinding on water-based abrasive papers (grade from 300 to 4000) and polishing with diamond pastes (9, 6, 3 and 1 μm). The microstructure was revealed by electroetching in a 40% nitric acid solution (etching time was from 5 to 15 seconds). The amount of ferrite was measured using an MPD-100A ferritometer from R&J Measurement. The device’s measuring range was from 0 to 100% of the magnetic phase in the volume of the material. The measurement was performed using a contact head, with the device’s measurement

accuracy being 0.1%. Measurement standards for austenitic steel with a magnetic phase share of up to 60% were applied. Ten measurements were made for each sample. Table 3 and 4 shows the mean value and measurement error.

## RESULTS

The results of diffraction tests (Figure 1a) show that steel in its initial state (0%) presents an almost single-phase austenitic structure.

In the diffractogram, apart from the lines coming from γ - austenite of (111)γ, (200)γ, (220)γ, (311)γ, and (222)γ, it is possible to observe a very weak (110)δ diffraction line coming from δ-ferrite. The volume fraction of ferrite (V<sub>F</sub>) calculated based on the (111) diffraction line for γ-austenite and (110)δ for δ-ferrite equaled approx. 2% of volume (formula 4) [45].

$$V_F = 1 - V_A = I - \frac{1.4 \frac{I_\gamma}{I_\alpha}}{1 + 1.4 \frac{I_\gamma}{I_\alpha}} \quad (4)$$

where: V<sub>A</sub> – volume fraction of austenite, I<sub>γ</sub> – total intensity of (111) diffraction line for austenite, I<sub>α</sub> – total intensity of (110) diffraction lines for ferrite.

The amount of ferrite measured with a ferritometer gave the result of 0.4% (Table 3). After 5% deformation, no significant changes in the diffraction pattern are observed. Starting from 20% deformation, there is a visible strengthening of the diffraction lines coming from the δ/α’ magnetic phase (the lines from δ - ferrite and

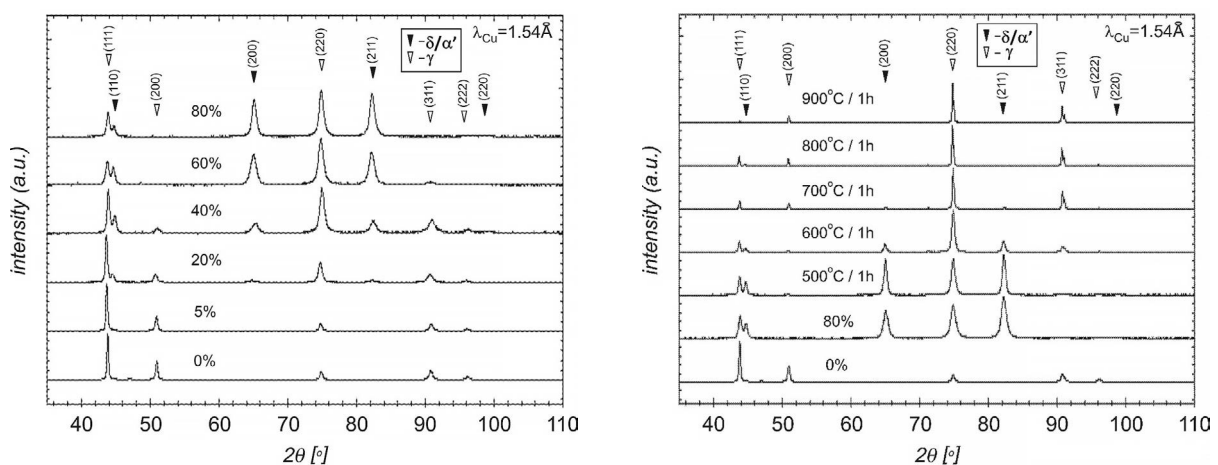


**Figure 1.** The X-Ray diffraction patterns of the steel: (a) in the initial state (0%) and after cold rolling 5–80% of deformation, (b) in the initial state (0%), after 80% of deformation and annealing at temperature 500–900 °C for 1 hour

**Table 3.** Volume fraction of magnetic phase  $\delta/\alpha'$  ( $\delta$ -ferrite and  $\alpha'$ -martensite) for steel in the initial state and after 5–80% deformation

$\varepsilon$ [%]	0	5	20	40	60	80
$V\alpha'$ [%]	0.4±0.1	0.5±0.1	6.1±0.2	18.1±0.1	28.6±0.2	38.4±0.4

$\alpha'$ -martensite have the same angular position  $2\theta$ , hence the marking in the diffractogram of  $\delta/\alpha'$ , while additional lines of  $(200)\delta/\alpha'$ ,  $(211)\delta/\alpha'$  and a faint line of  $(220)\delta/\alpha'$  appear. This proves that  $\gamma \rightarrow \alpha'$  martensitic transformation occurs in steel as a result of deformation. The SFE of austenite estimated on the basis of its chemical composition is low ( $17.13 \text{ mJ/m}^2$ ), thus, three deformation mechanisms are possible: partial dislocation slip, twinning and deformation-induced phase transformation. The calculated temperature of  $M_{d30/50}$  for the tested steel is approx.  $41 \text{ }^\circ\text{C}$ , and the steel was deformed at a lower temperature (room temperature), which also favors the occurrence of phase transformation during deformation. The results of diffraction tests indicate that the transformation takes place by direct transformation of austenite into martensite with the regular structure  $\gamma \rightarrow \alpha'$  and there is no martensite with a hexagonal structure as an intermediate phase  $\gamma \rightarrow \varepsilon \rightarrow \alpha'$ .

Research conducted by Li et al. [46] on 316L steel shows that lowering the deformation temperature causes a decrease in austenite stability and, during deformation by stretching steel at low temperatures, lines originating from the  $\varepsilon$  phase are observed in the diffractograms as a transition phase in the transformation of austenite into  $\alpha'$ -martensite. However, Padilha et al. [25], testing AISI 304 austenitic steel after deformation by cold rolling, showed that  $\varepsilon'$ -martensite formed in steel but at low degrees of deformation up to 5% and then, with an increase in the degree of deformation, it was transformed into  $\alpha'$ -martensite.  $\varepsilon$ -martensite as an intermediate phase is also observed in high-manganese austenitic steels [16, 17, 47]. For the tested steel, there are no diffraction lines from the  $\varepsilon$  phase in the entire range of deformations of 5–80%, which confirms that the phase transformation in this steel occurs along the  $\gamma \rightarrow \alpha'$  path. Magnetic tests indicate an increase in the volume fraction of the magnetic phase with an increase in the degree of deformation. After 80% deformation, the volume fraction was about 38% (Table 3).

In the diffractogram of steel annealed at  $500 \text{ }^\circ\text{C}$  for 1 hour, no significant changes in the diffraction pattern are observed. There are only

differences in intensity for individual lines. Starting from the annealing temperature of  $600 \text{ }^\circ\text{C}$ , clear changes are visible in the diffractograms. The diffraction lines from the phase  $\delta/\alpha'$  are weakened, which is the result of the reverse transformation of  $\alpha'$ -martensite into  $\gamma$ -austenite. In the diffractogram of the sample after annealing at  $900 \text{ }^\circ\text{C}$  for 1 hour, the lines originating from the magnetic phase  $\delta/\alpha'$  practically disappear (Figure 1b). The tests carried out on the volume fraction of the magnetic phase measured using a ferritometer indicate that, already after annealing at the temperature of  $800 \text{ }^\circ\text{C}$ , a complete reverse transformation  $\alpha' \rightarrow \gamma$  took place (Table 4).

Differences of 0.1% for the initial state compared to the state after annealing at 800 and  $900 \text{ }^\circ\text{C}$  may result from a measurement error of this method. The analysis of the full width at half maximum (FWHM) for individual lines originating from austenite is presented in Figure 2. As the annealing temperature increases, the full width at half maximum decreases, which proves that the reverse transformation takes place by diffusion.

The reverse transformation was studied, for example, by Tomimura et al. [36] for two austenitic steels, 15.6Cr-9.8Ni and 17.6Cr-8.8Ni. They demonstrated that annealing steel at the temperature of  $400 \text{ }^\circ\text{C}$  did not lead to the reverse transformation  $\alpha' \rightarrow \gamma$ . Only heating to  $650 \text{ }^\circ\text{C}$  led to a reverse transformation, with a different transformation path depending on the chemical composition: by shearing (15.6Cr-9.8Ni steel) or by diffusion (17.6Cr-8.8Ni steel). If the transformation took place by shearing, the austenite formed after the transformation has a high dislocation density [36]. If the defect density increases, it leads to a broadening of the diffraction lines. A decrease in FWHM was recorded in the tested steel,

**Table 4.** Volume fraction of magnetic phase  $\delta/\alpha'$  ( $\delta$ -ferrite and  $\alpha'$ -martensite) for steel after 80% deformation and annealing at temperature at 500–900  $^\circ\text{C}$  for 1 hour

Annealing temperature	500 $^\circ\text{C}$	600 $^\circ\text{C}$	700 $^\circ\text{C}$	800 $^\circ\text{C}$	900 $^\circ\text{C}$
$V\alpha'$ [%]	33.2±0.3	7.5±0.2	0.7±0.1	0.5±0.1	0.3±0.2

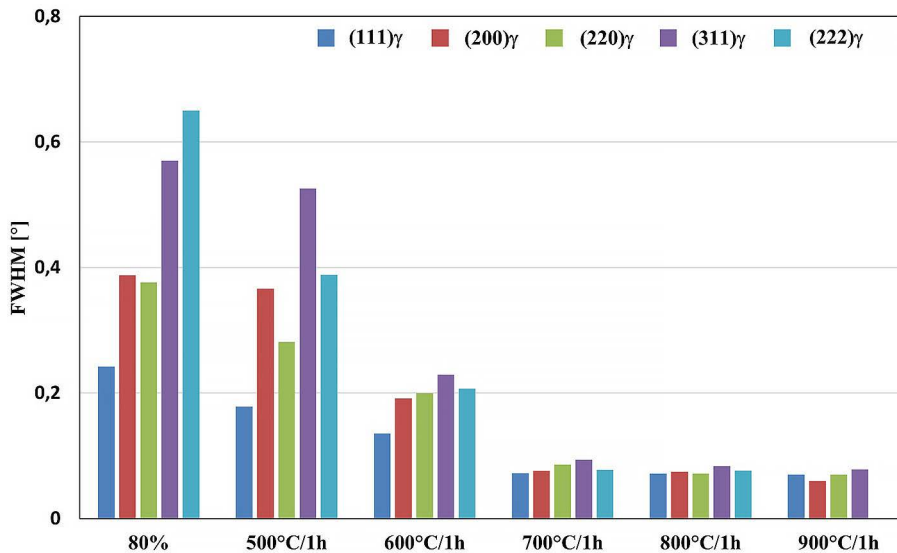


**Figure 2.** Changes in full width at half maximum (FWHM) for samples after 80% deformation and annealing at 500–900 °C for planes originating from austenite ( $\gamma$ -phase)

confirming the diffusive nature of the reverse transformation (Figure 2). Table 4 shows changes in the volume fraction of the magnetic phase depending on the heat treatment temperature. It can be seen that the most intense transformation took place in the temperature range of 500–600 °C.

Figure 3 shows the ideal orientations and orientation fibers that occur in metals and alloys with a regular structure (BCC and FCC) to facilitate the analysis of the crystallographic texture of

the tested steel samples after deformation and annealing (Figures 4–9).

Austenite texture in the initial state (Figures 3, 4, 6 and 9a) had a poor, almost random orientation. The maximum value of ODF = 1.8 corresponded to the  $\{100\} \langle 001 \rangle$  orientation. After 5% deformation, the austenite still had a random orientation. The maximum ODF value shifted to the  $\{001\} \langle 510 \rangle$  orientation. Starting from 20% deformation, austenite begins to show a fibrous character. The texture shows a weak fiber  $\alpha =$

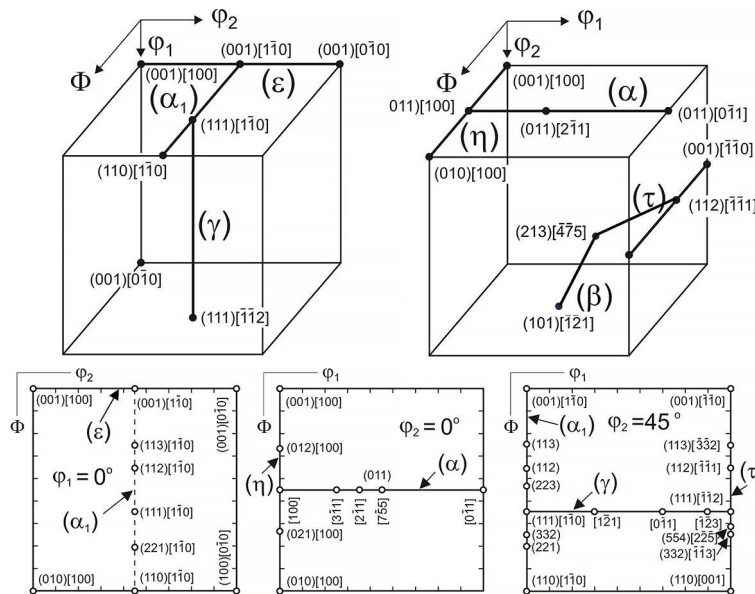


**Figure 3.** The ideal orientations and orientation fibers which occur in the texture of metals and alloys with BCC ( $\alpha_1 = \langle 110 \rangle \parallel \text{RD}$ ,  $\gamma = \langle 111 \rangle \parallel \text{ND}$  and  $\varepsilon = \langle 001 \rangle \parallel \text{ND}$ ) and FCC ( $\alpha = \langle 110 \rangle \parallel \text{ND}$ ,  $\eta = \langle 001 \rangle \parallel \text{RD}$ ,  $\tau = \langle 110 \rangle \parallel \text{TD}$  and  $\beta$ ) structures presented in the Euler space and on the cross sections  $\phi_1 = 0^\circ$ ,  $\phi_2 = 0^\circ$  and  $\phi_2 = 45^\circ$

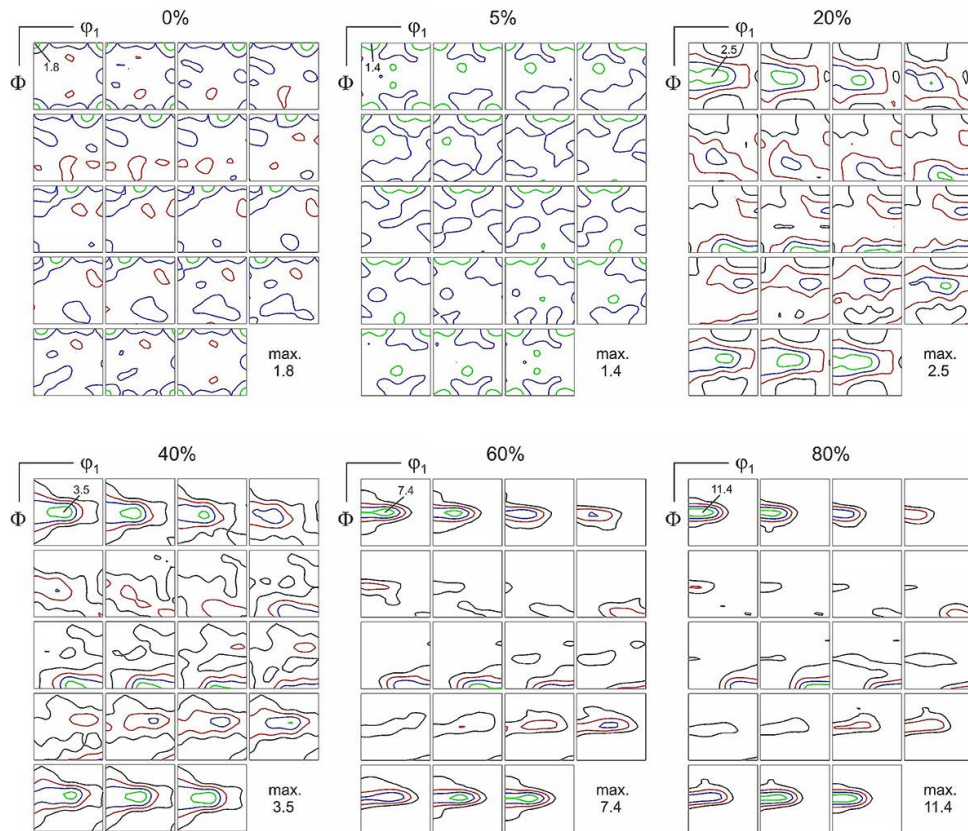


**Figure 4.** Orientation distribution function (ODFs) for austenite in the initial state (0%) and after deformation 5–80%

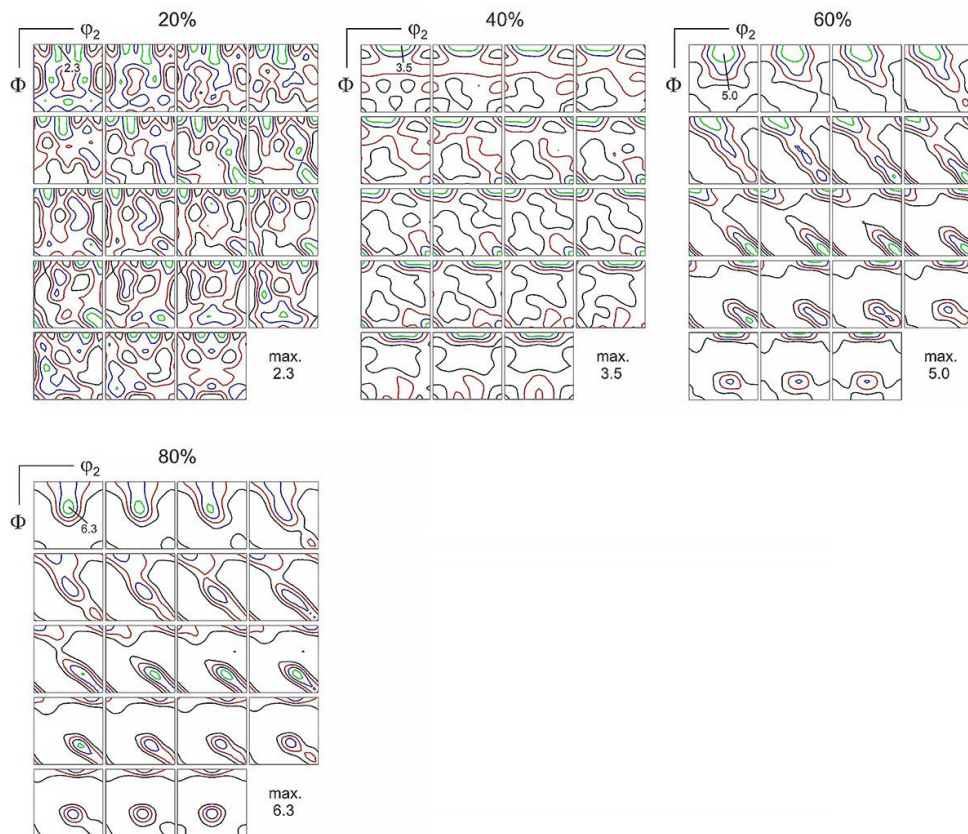


**Figure 5.** Orientation distribution function (ODFs) for martensite in the samples after deformation 20–80%

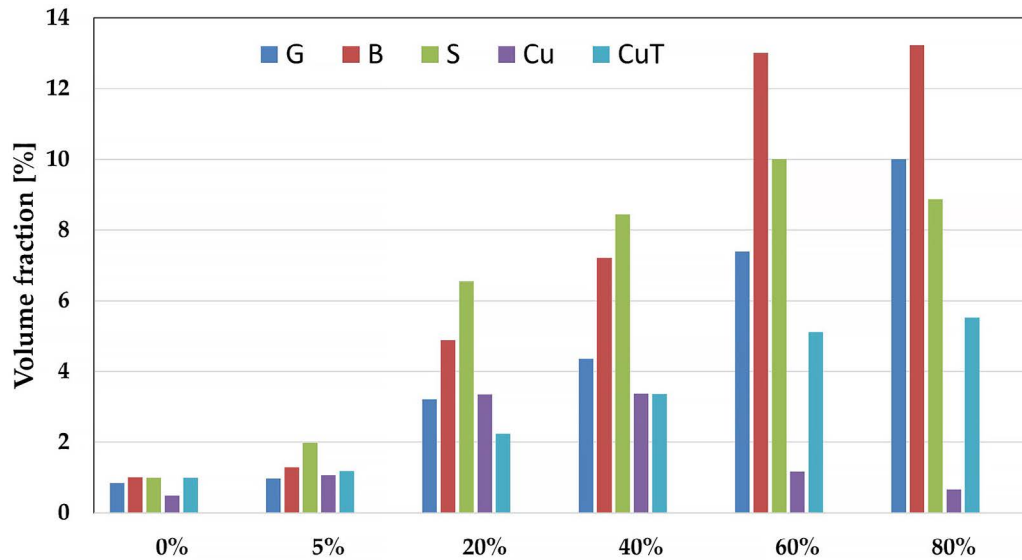


**Figure 6.** The calculated volume fractions of the important crystallographic orientation that occur in texture of austenite after deformation (orientation: G –  $\{110\}\langle 001\rangle$ , B –  $\{110\}\langle 112\rangle$ , S –  $\{123\}\langle 364\rangle$ , Cu –  $\{112\}\langle 111\rangle$ , CuT –  $\{552\}\langle 115\rangle$ )



**Figure 7.** Orientation distribution function (ODFs) for austenite after 80% deformation and annealing at temperature 500–900 °C for 1 hour

$\langle 110\rangle$ IND with a maximum for the  $\{110\}\langle 112\rangle$  orientation (B-brass type). As the degree of deformation increased, so did the degree of texturing. The  $\alpha$  fiber orientation was strengthened with a maximum corresponding to the  $\{110\}\langle 112\rangle$ ,

$\{110\}\langle 113\rangle$  and  $\{110\}\langle 115\rangle$  orientations, respectively, for the deformation of 40, 60 and 80%. The Goss-type  $\{110\}\langle 001\rangle$  orientation is strong throughout the entire range of deformations. In the texture of deformed austenite there

are also weak orientations, such as  $\{113\}\langle 332\rangle$ ,  $\{123\}\langle 364\rangle$  (S-type) and  $\{112\}\langle 111\rangle$  (Cu-type). As the degree of deformation increases, an increase in the CuT  $\{552\}\langle 115\rangle$  component is observed (Figures 3, 4, 6, and 9a). This is caused by mechanical twinning occurring in austenite. This is evidenced by a decrease in the volume fraction of the Cu-type component and an increase in the volume fraction of the CuT  $\{552\}\langle 115\rangle$  component (Figure 6). This is confirmed by literature data [23, 40] according to which Cu-type orientation, which appears during smaller degrees of deformation, undergoes a transformation as a result of twinning into the CuT orientation, and then as a result of slippage into the Goss  $\{110\}\langle 001\rangle$  orientation, which rotates in the direction of the  $\{110\}\langle 112\rangle$  orientation.

The volume fraction of  $\delta$  phase (ferrite) and  $\alpha'$  phase (martensite) for the material in its initial state and after deformation of 5% is approximately 0.5%, which made it impossible to measure the crystallographic texture. After 20% deformation, the volume fraction of the magnetic phase increases (Table 3), leading to an attempt being made to measure the martensite texture.

For this degree of deformation, it is almost random and it can be observed that the  $\alpha'$ -martensite texture has a partially fibrous character only after 40% deformation. The texture is dominated by orientations belonging to the  $\alpha_1 = \langle 110\rangle \parallel \text{RD}$ ,  $\varepsilon = \langle 001\rangle \parallel \text{ND}$  fiber and the maximum ODF value corresponds to the  $\{010\}\langle 403\rangle$  orientation. As the deformation increases to 80%, the degree of martensite texturing increases (max. value of ODF=6.3). The orientation fibers become stronger. The ODF value for the  $\{332\}\langle 113\rangle$  orientation increases and for 80% deformation equals 5.6. However, the maximum ODF value corresponds to the  $\{112\}\langle 110\rangle$  orientation and belongs to the  $\alpha_1$  orientation fiber (Figures 3, 5 and 9b).

After annealing at 500 °C, no significant changes in the crystallographic texture of either austenite or martensite were observed (Figures 7–9). The maximum ODF value in fiber  $\alpha$  shifted to the  $\{110\}\langle 113\rangle$  orientation. As the annealing temperature increased,  $\alpha$  fiber became spread. The degree of austenite texturing also decreases. After annealing at 800 °C, the maximum ODF value shifted to the Goss  $\{110\}\langle 001\rangle$  orientation (Figures 7 and 9a).

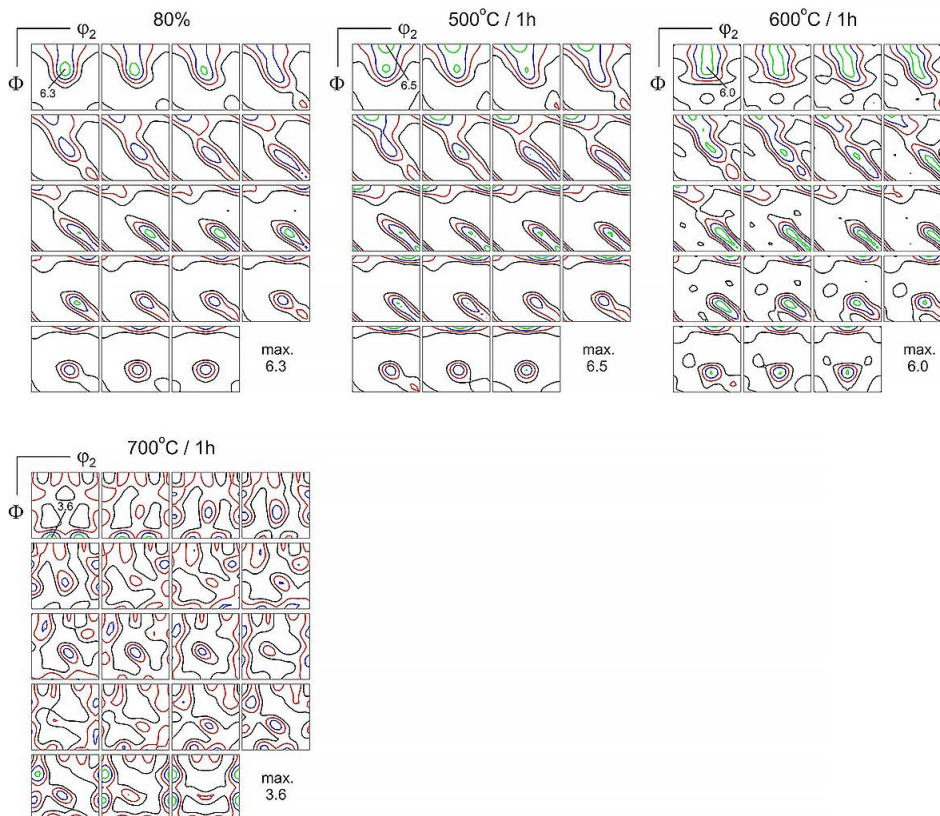


**Figure 8.** Orientation distribution function (ODFs) for  $\alpha'$ -martensite after 80% deformation and annealing at temperature 500–700 °C for 1 hour

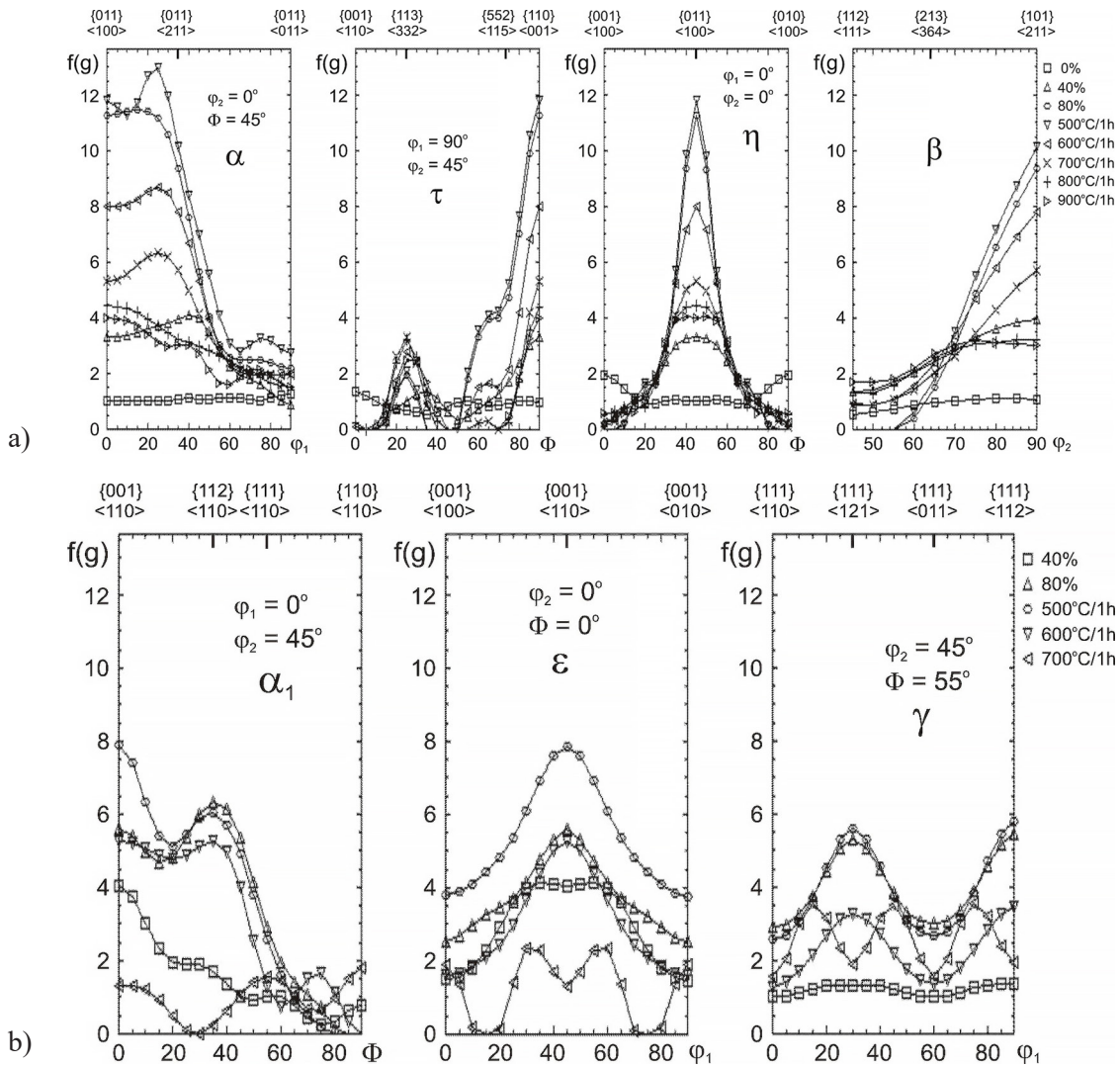


**Figure 9.** Value of the orientation distribution functions  $f(g)$  along the orientation fibers  $\alpha = \langle 110 \rangle \parallel \text{IND}$ ,  $\eta = \langle 001 \rangle \parallel \text{RD}$ ,  $\tau = \langle 110 \rangle \parallel \text{TD}$  and  $\beta = \{110\} \langle 112 \rangle$  via  $\{123\} \langle 364 \rangle$  to  $\{112\} \langle 11 \rangle$  for the  $\gamma$ -austenite phase (a) and  $\alpha_1 = \langle 110 \rangle \parallel \text{RD}$ ,  $\gamma = \langle 111 \rangle \parallel \text{IND}$  and  $\epsilon = \langle 001 \rangle \parallel \text{IND}$  for the  $\alpha'$ -martensite phase (b). Samples for the initial state (0%), after selection rolling reductions (40%, 80%) and after annealing at 500–900 °C

After annealing at 500 °C, the intensity of orientations lying in the orientation fibers  $\alpha_1$ ,  $\epsilon$  and  $\gamma$  for  $\alpha'$ -martensite increases slightly. This is related to the ongoing recovery processes. The maximum ODF value shifted to the  $\{001\} \langle 110 \rangle$  orientation. The value of the  $\{111\} \langle 112 \rangle$  texture component also increased. After annealing at 600 °C, the fiber  $\alpha_1$  became spread. The orientations belonging to this fiber also weakened. After annealing at 700 °C, the volume fraction of martensite in steel decreases significantly, which is reflected in a significant decrease in the degree of martensite texturing and a weakening of the main orientations (Figures 8 and 9b). After annealing at higher temperatures of 800 and 900 °C, it was not possible to measure the texture due to the small volume fraction of this phase (phase  $\delta/\alpha'$  – Table 4). Equiaxed

austenite grains of various sizes are observed in the microstructure of the steel in its initial state (Figure 10a). Dark bands indicate some share in the structure of  $\delta$ -ferrite. This is confirmed by previous X-ray and magnetic studies (Figure 1, Table 3). As the degree of deformation increases to 20%, darker etched areas in the austenite grains can be observed in the structure-deformation bands, which are privileged places for deformation-induced martensite nucleation (Figure 10b). As the deformation increases, so does the banding of the structure and characteristic ripples can be observed (Figures 10c and 10d). In the microstructure of steel after annealing at 500 °C, no significant changes are observed and the band character is preserved (Figure 11a). After annealing at 600 °C for 1 hour, the band microstructure is still

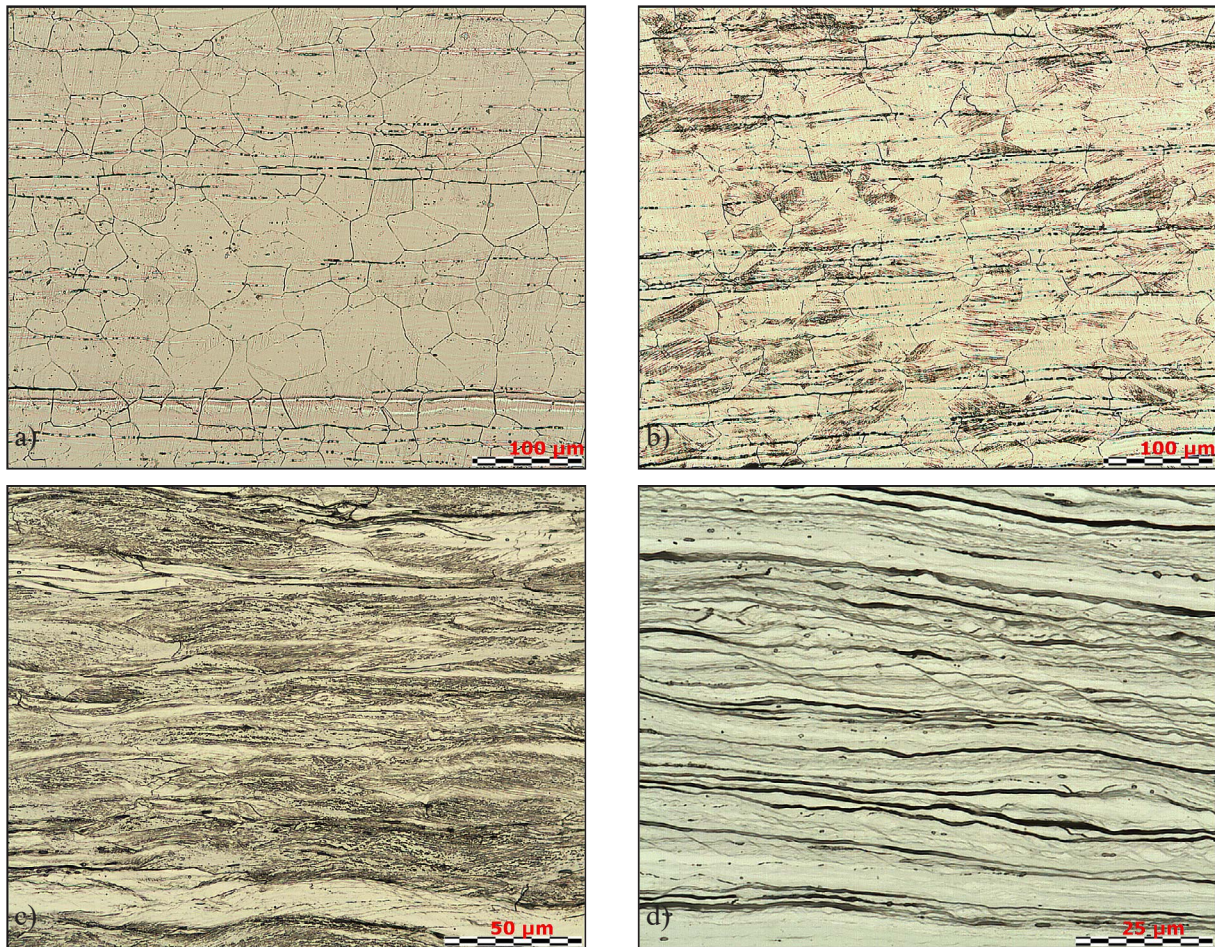


**Figure 10.** Microstructure of the steel in the initial state (a) and after selected rolling reduction: 20% (b), 60% (c) and 80% (d)

preserved, but the beginnings of the recrystallization process are observed (Figure 11b). Increasing the annealing temperature to 700 °C leads to an already recrystallized structure being obtained (Figure 11c), and austenite grains already grow when annealing steel at 900 °C (Figure 11d). This is reflected in a significant decrease in the degree of austenite texturization.

## DISCUSSION

The performed X-ray tests indicate that the texture development of the tested austenitic steel is complex, which is related to several different processes occurring simultaneously in steel, both during deformation and annealing. As a result of cold processing, austenite is texturized and transformed into martensite ( $\gamma \rightarrow \alpha'$ ), maintaining specific crystallographic relationships between phases and the development of martensite texture previously formed as a result of deformation. The

texture of the tested steel is therefore described by the components of two phases,  $\gamma$ -austenite and  $\alpha'$ -martensite. The deformed austenite texture is dominated by orientations belonging to the  $\alpha = \langle 110 \rangle \parallel \text{ND}$  fiber with strong Goss  $\{110\} \langle 001 \rangle$  and alloy  $\{110\} \langle 112 \rangle$  orientations.  $\{111\} \langle uvw \rangle$  components were also observed in the deformed austenite texture, proving the influence of mechanical twinning on the obtained texture of deformed austenite. Figure 12 shows the transformation of the experimental martensite orientation distribution function after 80% deformation according to the Kurdjumov-Sachs ( $\alpha \rightarrow \gamma_{\text{K-S}}$ ) and Nishiyama-Wassermann ( $\alpha \rightarrow \gamma_{\text{N-W}}$ ) relationships. Comparison of the ODF of austenite after 80% deformation and the ODF obtained after transformations ( $\alpha \rightarrow \gamma_{\text{K-S}}$  and  $\alpha \rightarrow \gamma_{\text{N-W}}$ ) indicates that these relationships suitably describe those between  $\gamma$ -austenite and  $\alpha'$ -martensite. It should be noted that these transformations were made

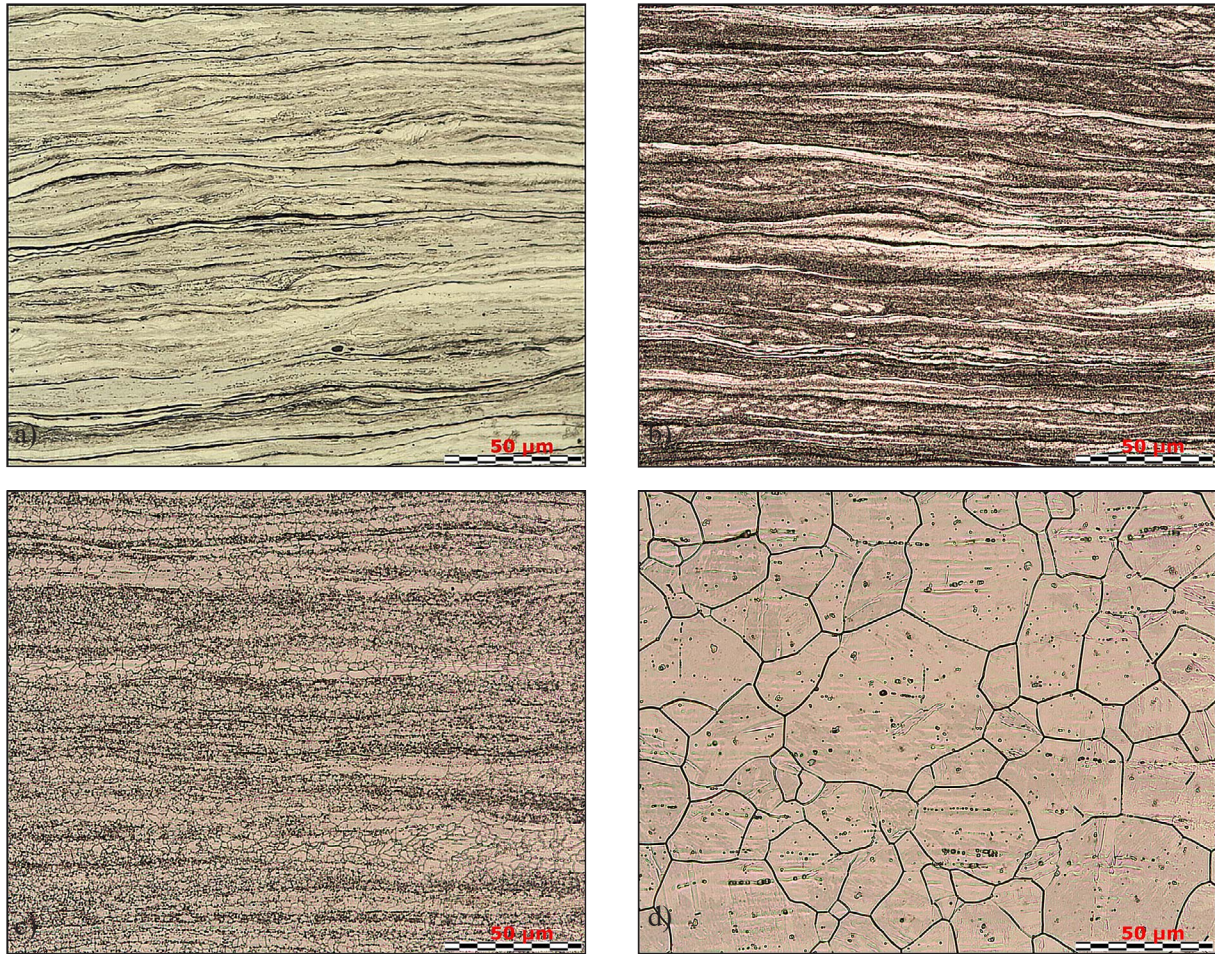


**Figure 11.** Microstructure of the steel after 80% deformation and annealing at 500 °C (a), 600 °C (b), 700 °C (c) and 900 °C (d) for 1 hour

without taking into account the variant selection, hence the ODF values are smaller.

The differences between the austenite texture after 80% deformation and that obtained after martensite transformation are also caused by the fact that we transformed the ODF of martensite obtained at a given stage of deformation, which consists of the martensite texture resulting from the  $\gamma \rightarrow \alpha'$  transformation as well as the texture of martensite previously deformed (at an earlier stage of rolling). In the deformed austenite texture, a strong component is the  $\{110\}\langle 112\rangle$  alloy orientation. The volume fraction of this texture component increased together with the degree of deformation, with a simultaneous increase in the volume fraction of the  $\{111\}\langle 112\rangle$  martensite component. However, as one work [48] states, the  $\{110\}\langle 112\rangle$  orientation of austenite transforms into the  $\{111\}\langle 112\rangle$  martensite component and the  $\{211\}\langle 111\rangle$  orientation of austenite transforms into the  $\{211\}\langle 011\rangle$  martensite orientation during deformation. Meanwhile, Ravi

Kumar et al. [24] found that the  $\{112\}\langle 110\rangle$  component of martensite was formed from the  $\{110\}\langle 001\rangle$  orientation of austenite, and the formation of the  $\{332\}\langle 113\rangle$  martensite component was linked with the  $\{110\}\langle 112\rangle$  orientation occurring in austenite. In the tested steel, both the Goss  $\{110\}\langle 001\rangle$  orientation and the alloy type  $\{110\}\langle 112\rangle$  show a high ODF value. The lack of the  $\{112\}\langle 111\rangle$  component in the austenite texture for the highest degrees of deformation can also be explained by the fact that, according to the K-S relationship, it changes to the  $\{112\}\langle 110\rangle$  martensite orientation [24, 25, 43].

Literature data indicate two mechanisms for the reverse transformation of martensite into austenite in steels. One occurs by shearing, the other by diffusion, and they depend on the chemical composition [34]. After annealing at 500 °C, no major changes in the intensity of martensite texture are observed. This can be explained by the improvement of the structure in this temperature range, and martensite is a stable phase at this

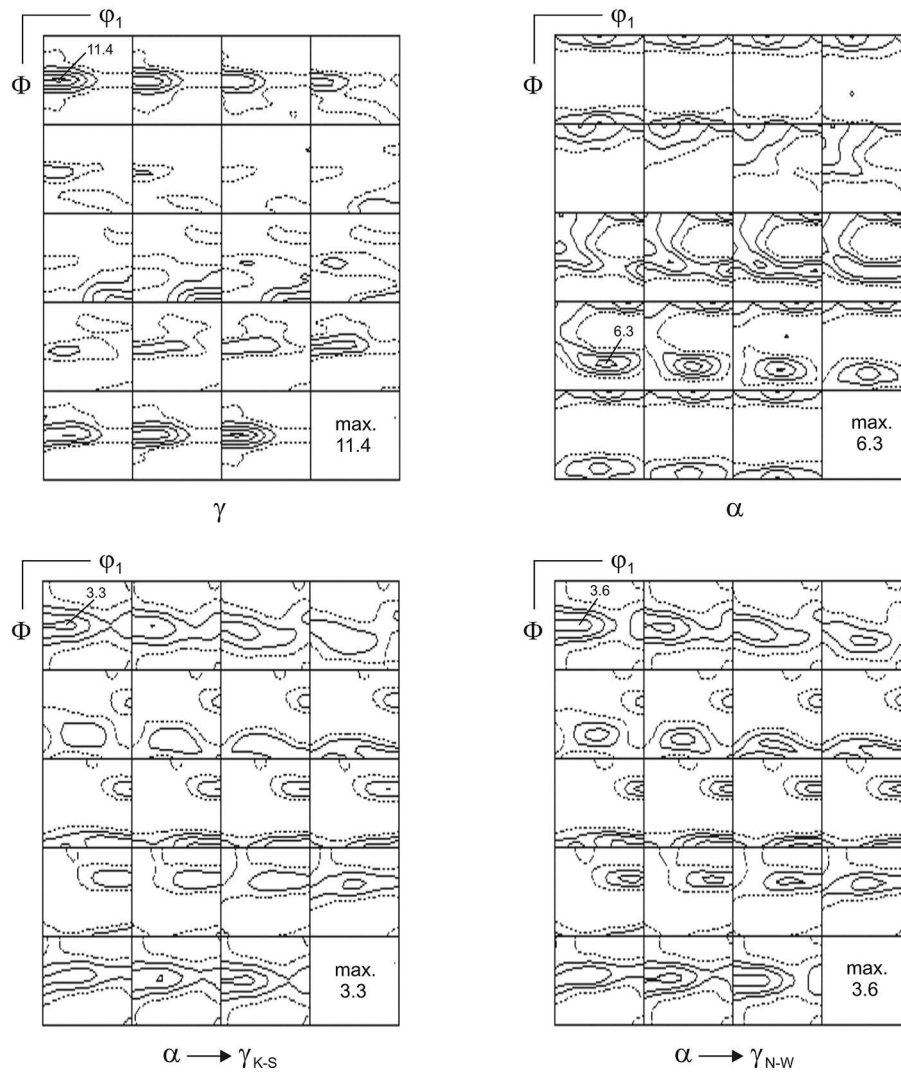


**Figure 12.** Experimental ODF values after 80% deformation for austenite ( $\gamma$ ) and  $\alpha'$ -martensite ( $\alpha$ ) and simulated transformations of martensite texture ( $\alpha' \rightarrow \gamma$ ) according to the Kurdjumov-Sachs ( $\alpha \rightarrow \gamma_{K-S}$ ) and Nishiyama-Wassermann ( $\alpha \rightarrow \gamma_{N-W}$ ) orientation relationships

annealing temperature. An increase in the annealing temperature led to a decrease in the volume fraction of the magnetic phase in the structure. The lack of an increase in full width at half maximum (FWHM) for lines originating from austenite for the tested steel indicates that the transformation takes place by diffusion. This is a different reverse transformation mechanism than that observed in [34] for 16Cr-10Ni steel. An increase in the annealing temperature led to a decrease in the percentage of  $\alpha'$ -martensite in the steel structure and then to a complete reverse transformation  $\alpha' \rightarrow \gamma$  (temperatures of 600 and 700 °C). The austenite annealing texture is a component of the annealing texture of the austenite that remained in the structure after the transformation and the texture of the austenite resulting from the transformation  $\alpha' \rightarrow \gamma$ . After annealing, an increase in the  $\{112\}\langle 111 \rangle$

component of austenite and a decrease in intensity for the  $\{113\}\langle 110 \rangle$  martensite component are observed. According to the K-S relation, this orientation transforms into the  $\{112\}\langle 111 \rangle$  and  $\{123\}\langle 111 \rangle$  orientations of austenite. Higher annealing temperatures result in a decrease in the degree of austenite texturing caused by the ongoing recrystallization processes, which is visible in the microstructure image. After annealing, the fibrous nature of the austenite texture is retained.

To sum up, it can be stated that the recovery process took place first during the annealing process (annealing temperature of 500 °C) for both phases, and then the phase transition  $\alpha' \rightarrow \gamma$  and recrystallization of the deformed austenite. The last stage was the growth of austenite grains, both obtained after transformation and after recrystallization.

## CONCLUSIONS

The results of diffraction and magnetic tests allow us to conclude that in the tested AISI 304 stainless steel, as a result of cold rolling, a deformation-induced transformation of austenite into martensite with a body-centered cube structure took place. During deformation, the austenite became texturized, and the  $\gamma \rightarrow \alpha'$  martensitic transformation occurred while maintaining specific crystallographic relationships between the phases, best described by the Kurdjumov-Sachs and Nishiyama-Wassermann relationships.

The reverse transformation of martensite into austenite in the tested steel occurred above a temperature of 500 °C. Decreasing of the full width at half maximum (FWHM) of diffraction lines coming from austenite for steel after annealing at temperatures above 500 °C confirms the diffusive nature of the reverse transformation. The sequence of processes occurring during annealing of the deformed AISI 304 steel was as follows:  $\alpha' \rightarrow \gamma$  reverse transformation, recrystallization of the deformed austenite, and grain growth of both austenites (obtained after both transformation and recrystallization).

## Acknowledgments

The authors also thank Krzysztof Chruściel for his support in this research. This research was funded by the AGH University of Krakow project number 16.16.110.663.

## REFERENCES

- Lamb S. ed. Casti Handbook of Stainless steel and nickel alloys, Publisher: CASTI Publishing Inc., Canada, 2000.
- Stainless Steel Market Size, Share & Trends Analysis Report By Grade (300 Series, Duplex Series), By Product (Flat, Long), By Application (Building & Construction, Consumer Goods), By Region, And Segment Forecasts, 2024-2030.
- Jeong J., Lee Y., Jeong Min Park J.M., Leec D.C., Jeond I., Sohnd H., Kimb H.S., Nama T.-H., Sunga H., Jae Bok Seola J.B., Jung Gi Kim J.G. Metastable  $\delta$ -ferrite and twinning-induced plasticity on the strain hardening behavior of directed energy deposition-processed 304L austenitic stainless steel. *Addit. Manuf.* 2021; 47: 102363. <https://doi.org/10.1016/j.addma.2021.102363>.
- Simmons J.W. High-nitrogen alloying of stainless steels. *Mater. Sci. Eng. A* 1996; 207: 159-69.
- Yuan Z.Z., Dai Q.X., Cheng X.N., Chen K.M., Pan L., Wang A.D. In situ SEM tensile test of high-nitrogen austenitic stainless steels. *Mater. Charact.* 2006; 56: 79–83. <https://doi.org/10.1016/j.matchar.2005.09.013>.
- Angel T. Formation of martensite in austenitic stainless steels effect of deformation, temperature and composition. *J. Iron and Steel Inst.* 1954; 177: 165–174.
- Ali S., Irfan M., Niazi U.M., Rani A.M.A., Rashedi A., Rahman S., Khan M.K.A., Alsaieri M.A., Legutko S., Petru J., Trefil A. Microstructure and mechanical properties of modified 316L stainless steel alloy for biomedical applications using powder metallurgy. *Materials.* 2022; 15: 2822. <https://doi.org/10.3390/ma15082822>.
- Maziasz P.J., Busby J.T. Properties of austenitic steels for nuclear reactor applications. *Comprehensive Nuclear Materials.* 2012; 2: 267–283. <https://doi.org/10.1016/B978-0-08-056033-5.00019-7>.
- Szala M., Beer-Lech K., Walczak M. A study on the corrosion of stainless steel floor drains in an indoor swimming pool. *Eng. Fail. Anal.* 2017; 77: 31–38. <http://dx.doi.org/10.1016/j.engfailanal.2017.02.014>.
- Walczak M. Surface characteristics and wear resistance of 316L stainless steel after different shot peening parameters. *ASTRJ* 2023; 17(3): 124–132. <https://doi.org/10.12913/22998624/165800>.
- Skoczylas A. Vibratory shot peening of elements cut with abrasive water jet. *ASTRJ.* 2022; 16(2): 39–49. <https://doi.org/10.12913/22998624/146272>.
- Padilha A.F., Rios P.R. Decomposition of austenite in austenitic stainless steels. *ISIJ Int.* 2002; 42(4): 325–337. <https://doi.org/10.2355/isijinternational.42.325>.
- Ganesh Sundara Raman S., Padmanabhan K.A. Tensile deformation-induced martensitic transformation in AISI 304LN austenitic stainless steel. *J. Mater. Sci. Lett.* 1994; 13: 389–392.
- Lecroisey F., Pineau A. Martensitic transformations induced by plastic deformation in the Fe-Ni-Cr-C system. *Metall. Trans.* 1972; 3: 387–396.
- Luo C., Yuan H. Measurement and modeling of deformation-induced martensitic transformation in a metastable austenitic stainless steel under cyclic loadings. *Acta Mater.* 2022; 238: 118202. <https://doi.org/10.1016/j.actamat.2022.118202>.
- Gräsel O., Krüger L., Frommeyer G., Meyer L.W. High strength Fe-Mn-(Al, Si) TRIP/TWIP steels development-properties-application. *Int. J. of Plast.* 2000; 16: 1391–1409. [https://doi.org/10.1016/S0749-6419\(00\)00015-2](https://doi.org/10.1016/S0749-6419(00)00015-2).
- Kowalska J., Rys J., Cempura G. Complex structural effects in deformed high-manganese steel. *Materials* 2021; 14(22): 6935. <https://doi.org/10.3390/>

- ma14226935.
18. Frommeyer G., Brück U., Neumann P. Supra-ductile and high-strength manganese - TRIP/TWIP steels for high energy absorption purposes. *ISIJ Int.* 2003; 43: 438–446. <https://doi.org/10.2355/isijinternational.43.438>.
  19. Braga D.P., Corrêa L.M., Sordi V.L., Rovere C.A.D., Cintho O.M., Kliuga A.M. Influence of temperature and stress state on the TWIP behavior of 201LN and 316LV austenitic stainless steels. *Mater. Sci. Eng. A.* 2023; 863: 144527. <https://doi.org/10.1016/j.msea.2022.144527>.
  20. Guo Y., Zhang S., Chen J., Fu B., Wang Z., Pang L., Wei L., Li Y., Ding Y. The contribution of retained martensite to the high yield strength and sustainable strain hardening of a hierarchical metastable austenitic stainless steel. *Mater. Sci. Eng. A.* 2023; 866: 144681. <https://doi.org/10.1016/j.msea.2023.144681>.
  21. Hu Ch., He Ch., Zhu X., Dong H., Wan X., Li G., Wu K. The significant role of bimodal lamellar heterostructure for Lüders deformation and TRIP effect in 18Cr–8Ni austenitic stainless steel. *Mater. Sci. Eng. A.* 2023; 887: 145748. <https://doi.org/10.1016/j.msea.2023.145748>.
  22. He Y., Gao J., He Y., Shin K. A new fcc-bcc orientation relationship observed in the strain-induced martensitic transformation of an austenitic stainless steel. *Mater. Lett.* 2021; 305: 130735. <https://doi.org/10.1016/j.matlet.2021.130735>.
  23. Ravi Kumar B., Mahato B., Bandyopadhyay N.R., Bhattacharya D.K. Comparison of rolling texture in low and medium stacking fault energy austenitic stainless steels. *Mater. Sci. Eng. A.* 2005; 394: 296–301. <https://doi.org/10.1016/j.msea.2004.11.057>.
  24. Ravi Kumar B., Singh A.K., Das S., Bhattacharya D.K. Cold rolling in AISI 304 stainless steel. *Mater. Sci. Eng. A.* 2004; 364: 132–139. <https://doi.org/10.1016/j.msea.2003.08.012>.
  25. Padilha A.F., Plaut R.L., Rios P.R. Annealing of cold-worked austenitic stainless steels. *ISIJ Int.* 2003; 43(2): 135–143. <https://doi.org/10.2355/isijinternational.43.135>.
  26. Hübner W. Phase transformations in austenitic stainless steels during low temperature tribological stressing. *Tribol. Int.* 2001; 34(4): 231–236. [https://doi.org/10.1016/S0301-679X\(01\)00006-8](https://doi.org/10.1016/S0301-679X(01)00006-8).
  27. Kowalska J., Ryś J., Cios G., Bednarczyka W. The effect of reduced temperatures on microstructure development in tensile tested high-manganese steel. *Mater. Sci. Eng. A.* 2018; 767: 138406. <https://doi.org/10.1016/j.msea.2019.138406>.
  28. Fang X.-H., Yang P., Lu F.-Y., Meng L. Dependence of deformation twinning on grain orientation and texture evolution of high manganese TWIP steels at different deformation temperatures. *J. Iron Steel Res. Int.* 2011; 18(11), 46–52. [https://doi.org/10.1016/S1006-706X\(11\)60116-7](https://doi.org/10.1016/S1006-706X(11)60116-7).
  29. Bokros J.C., Parker E.R. The mechanism of the martensite burst transformation in Fe Ni single crystals. *Acta Metall.* 1963; 11(12): 1291–1301. [https://doi.org/10.1016/0001-6160\(63\)90024-5](https://doi.org/10.1016/0001-6160(63)90024-5).
  30. Higo Y., Lecroisey F., Mori T. Relation between applied stress and orientation relationship of  $\alpha'$  martensite in stainless steel single crystals. *Acta Metall.* 1974; 22(3), 313–323. [https://doi.org/10.1016/0001-6160\(74\)90170-9](https://doi.org/10.1016/0001-6160(74)90170-9).
  31. Byun T.S., Hashimoto N., Farrell K. Temperature dependence of strain hardening and plastic instability behaviors in austenitic stainless steels. *Acta Mater.* 2004; 52 (13): 3889–3899. <https://doi.org/10.1016/j.actamat.2004.05.003>.
  32. Spencer K., Embury J.D., Conlon K.T., Véron M., Bréchet Y. Strengthening via the formation of strain-induced martensite in stainless steel. *Mater. Sci. Eng. A.* 2004; 387-389: 873–881. <https://doi.org/10.1016/j.msea.2003.11.084>.
  33. Tavares S.S.M., Gunderov D., Stolyarov V., Neto, J.M. Phase transformation induced by severe plastic deformation in the AISI 304L stainless steel. *Mater. Sci. Eng. A.* 2003; 358: 32–36. [https://doi.org/10.1016/S0921-5093\(03\)00263-6](https://doi.org/10.1016/S0921-5093(03)00263-6).
  34. Tomimura K., Takaki S., Tokunaga Y. Reversion mechanism from deformation induced martensite to austenite in metastable austenitic stainless steel. *ISIJ Int.* 1991; 31(12): 1431–1437. <https://doi.org/10.2355/isijinternational.31.1431>.
  35. Bunsch A., Kowalska J., Chruściel K. Texture and microstructure of annealed AISI 302 steels wire. *Arch. Metall. Mater.* 2008; 53(1): 125–130.
  36. Tomimura K., Takaki S., Tanimoto S. Optimal chemical composition in Fe-Cr-Ni alloys for ultra grain refining by reversion from deformation induced martensite. *ISIJ Int.* 1991; 31(7): 721–727. <https://doi.org/10.2355/isijinternational.31.721>.
  37. Martins L.F.M., Plaut R.L., Padilha A.F. Effect of carbon on cold-worked state and annealing behaviour of two 18wt%Cr-8wt%Ni austenitic stainless steels. *ISIJ Int.* 1998; 38(6): 572–579. <https://doi.org/10.2355/isijinternational.38.572>.
  38. Tavares S.S.M., Fruchart D., Miraglia S. A magnetic study of the reversion of martensite  $\alpha'$  in a 304 stainless steel. *J. Alloys Compd.* 2000; 307: 311–317. [https://doi.org/10.1016/S0925-8388\(00\)00874-4](https://doi.org/10.1016/S0925-8388(00)00874-4).
  39. Takaki S., Tomimura K., Ueda S. Effect of pre-cold-working on diffusional reversion of deformation in metastable austenitic stainless steel. *ISIJ Int.* 1994; 34(6): 522–527. <https://doi.org/10.2355/isijinternational.34.522>.
  40. Heye W., Wassermann G. The formation of the rolling textures of FCC metals by slip and twinning,

- Scripta Metall. 1968; 2: 693-697. [https://doi.org/10.1016/0036-9748\(68\)90228-7](https://doi.org/10.1016/0036-9748(68)90228-7).
41. Chowdhury S.G., Das S., Ravi Kumar B., Kumar S., Gottstein G. Textural development in AISI 316 stainless steel during cold rolling and annealing. *Materials Science Forum* 2002; 408-412: 1371–1376. DOI:10.4028/WWW.SCIENTIFIC.NET/MSF.408-412.1371
42. Donadille C., Valle R., Dervin P., Penelle R. Development of texture and microstructure during cold-rolling and annealing of FCC alloys: Example of austenitic stainless steel. *Acta Metall.* 1989; 37(6): 1547-1571. DOI:10.1016/0001-6160(89)90123-5.
43. Raabe D. Texture and microstructure evolution during cold rolling of a strip cast and of hot rolled austenitic stainless steel. *Acta Mater.* 1997; 45(3): 1137–1151. [https://doi.org/10.1016/S1359-6454\(96\)00222-4](https://doi.org/10.1016/S1359-6454(96)00222-4).
44. Nie Z., Li Y., Wang Y. Mechanical properties of steels for cold-formed steel structures at elevated temperatures. *Adv. Civ. Eng.* 2020; ID 9627357: 1-18. <https://doi.org/10.1155/2020/9627357>.
45. Skrzypek S.J., Bergmark A., Góly M. Structural characterization of surface layers in sintered DistaloyAE and DistaloyHP. *Mater. Eng.* 2013; 4 (194): 370–373.
46. Li S., Withers P.J., Kabra S., Yan K. The behaviour and deformation mechanisms for 316L stainless steel deformed at cryogenic temperatures. *Mater. Sci. Eng. A.* 2023; 880: 145279. <https://doi.org/10.1016/j.msea.2023.145279>.
47. Ma D.D., Yang P., Gu X.F., Cui F. Influences of initial microstructures on martensitic transformation and textures during cold rolling and tensile mechanical properties in high manganese TRIP steel. *Mater. Sci. Eng. A.* 2022; 829: 142147. <https://doi.org/10.1016/j.msea.2021.142147>.
48. Yushkov V.I., Adamescu R.A., Machnev Y.S., Gapeka T.M., Geld P.V. The developments in texture in stainless steel. *Mater. Sci. Eng.* 1984; 64: 157–169.